Draft version December 15, 2024
Typeset using LaTeX **twocolumn** style in AASTeX631

Determining the distance, spectral type, temperature, and mass of the variable star DY Pegasi

Aaron Burke[1]

[1]*Department of Physics and Astronomy, Stony Brook University, Stony Brook, NY 11794, USA*

ABSTRACT

We observe 3 periods of the SX Phoenicis variable DY Pegasi using the 14" telescope at the Mt. Stony Brook Observatory. We take 518 images over 6 hours on the night of October 28, 2022 using the STL-1001E CCD camera in both the B and V filters. We find its period to be 0.072918 ± 0.000024 d using `PIPS`, a Python pipeline designed to analyze light curves. We determined its distance to be 343 ± 24 pc using the known SX Phoenicis variable Period-Luminosity Relation from R. Cohen et al. We concatenate a B-V color index curve and determine its spectral type to vary between A6.5–A9.5. We find its temperature to vary between $[7401, 8242]$ K. We estimate its mass to be approximately 1.3 $M_\odot$. These results are consistent with the literature on DY Pegasi.

1. INTRODUCTION

SX Phoenicis variable stars are a classification of variable stars characterized by their short periods (< 0.1 d), large amplitudes (> 0.2 mag), and low metallicity (Pop. II stars). They tend to be A-type stars, and often exist as blue stragglers of a globular cluster (Xue & Niu 2020). Blue stragglers are stars in a globular cluster that are brighter and bluer than the turnoff point of the cluster. The conditions that give rise to their formation are not well understood, but one theory is that they arise from a mass exchange or even stellar collision, allowing the star to be more massive, more luminous, and bluer than other constituents of the globular cluster (Rodríguez & López-González 2000). SX Phoenicis variables are a type of pulsating variable, meaning their variability in magnitude arises from the star's radius expanding and contracting over the duration of the period (i.e. radial pulsation). They are often grouped up with Delta Scuti variables, which are also short period, large amplitude variables, but have typical metallicities (Pop. I). There is a known period-luminosity relation for SX Phoenicis variables (Cohen & Sarajedini 2011).

DY Pegasi is one such SX Phoenicis variable. It is known to have a short period ($0.07292621 \pm 0.00000005$ d) and large amplitude (≈ 0.6 mag) from Xue & Niu (2020). It also has a low metallicity ([Fe/H] $= -0.8$) from Hintz et al. (2004). It has a spectral type of A that varies throughout the course of its period. Notably, it is one of the SX Phoenicis stars that lie in the general star field (not in a globular cluster), located at $23^{\mathrm{h}}\ 08^{\mathrm{m}}\ 51^{\mathrm{s}}$ $+17^\circ\ 12'\ 56''$. DY Pegasi is also one of the brighter SX Phoenicis stars visible with V ≈ 10.3. As a result of its location in the general star field, northern hemisphere visibility, and its brightness, it is well studied and there is a fair amount of literature on it. SX Phoenicis variables, like Delta Scuti variables, can be used as a standard candle to determine distances to other stars. Since most SX Phoenicis variables are in globular clusters, identifying candidate stars in those globular clusters and determining their distance would provide a distance estimate to the globular cluster.

Our primary objective was to concatenate a light curve of 3 periods of DY Pegasi over 1 night. We then determined the period from this light curve, used the period-luminosity relation to find its absolute visual magnitude, and determined its distance from Earth using the distance modulus. We took observations alternating from the B band to the V band about every 5 minutes. We can fit a curve to both of these bands separately. Thus, we had a secondary objective of creating a B–V color index curve. From the B–V color index, we can obtain a spectral type using tables from Fitzgerald (1970). B–V color index can also be converted to the star's effective temperature using a formula from Ballesteros (2012). Finally, we plot the star's luminosity vs. temperature over time. By overlaying several stellar evolution tracks from Georgy et al. (2013), we can roughly estimate DY Pegasi's mass. In section 2, we explain our data acquisition and data. In section 3, we calibrate and correct our data. In section 4, we obtain the period, distance, color index, temperature, and mass of DY Pegasi. We conclude in section 5 and acknowledge in section 6.

2. DATA

We observed DY Pegasi using the 14-inch LX200-ACF telescope and STL-1001E CCD camera at Mt. Stony Brook Observatory. We took our observations on the

night of October 28, 2022. The weather was clear with no clouds in the area. There was little to no wind, and it was nearly a new moon. DY Pegasi would remain above 30° altitude in the night sky from sunset until about 2:00 AM.

Throughout the night, we took 30 s exposures. This is the maximum reasonable exposure without noticable tracking errors. Although the telescope tracked the night sky, it isn't perfect and there is a slight drift over time; exposures longer than 30 s would begin to show signs of this drift. Starting at 7:40 PM local time, we began a series of 10 exposures (5 min cumulative) in the V band. Next, we switched to the B filter, and took 10 exposures in the B band. Then, we switched back to the V filter. We alternated between the two filters until 2:00 AM. There is a 15 minute gap in observations starting at about 10:00 PM as this was when we performed a meridian flip of the telescope. In total, we obtained 518 images of DY Pegasi. See Table 1 for a summary of these observations. We also took a series of 10 dark frames for the science images, 10 V filter dome flats, and 10 B filter dome flats. We also took 10 darks for the V dome flats and 10 darks for the B dome flats (the two series of flats had different exposure times). We had to take flats for the different filters as the dust pattern on the two filters is different.

Table 1. Table of Observations

Series	Filter	Image #	UTC Start
1	V	0–9	23:40
2	B	10–19	23:46
3	V	20–29	23:52
4	B	30–39	23:58
⋮	⋮	⋮	⋮
20	V	200–209	01:54
21	B	210–219	02:15
⋮	⋮	⋮	⋮
50	V	500–509	05:48
51	B	510–519	05:55

The 30 s exposure time was adequate for our observations. We want to avoid surpassing 40000 counts as the pixels would begin to saturate, but also keep the counts as high as possible to get the largest signal-to-noise ratio. Also note that our counts in the B band were lower than the V band in general, likely due to a lower overall throughput at blue wavelengths. Our maximum counts in any pixel for DY Peg reached about 35000 at its maximum in the V band, and 8000 at its minimum in the B band. This is a good range, as it avoids the saturation limit and maintains a high signal-to-noise ratio at its dimmest point of its period in the B band.

DY Pegasi is the second brightest star in our exposures, with V ≈ 10.3. HD 218587 is the brightest non-variable star at V ≈ 9.8, B ≈ 10.4 (Henden et al. 2015). This star ends up exceeding 40000 counts in the V band, with counts upwards of 45000. Hence, we avoid using it for our visual magnitude calibration. However, it is fine to use for the blue magnitude calibration. We use the star GSC 01712-00542 with V ≈ 11.9, B ≈ 12.4 to calibrate for the V magnitude. These stars are highlighted in Figure 1.

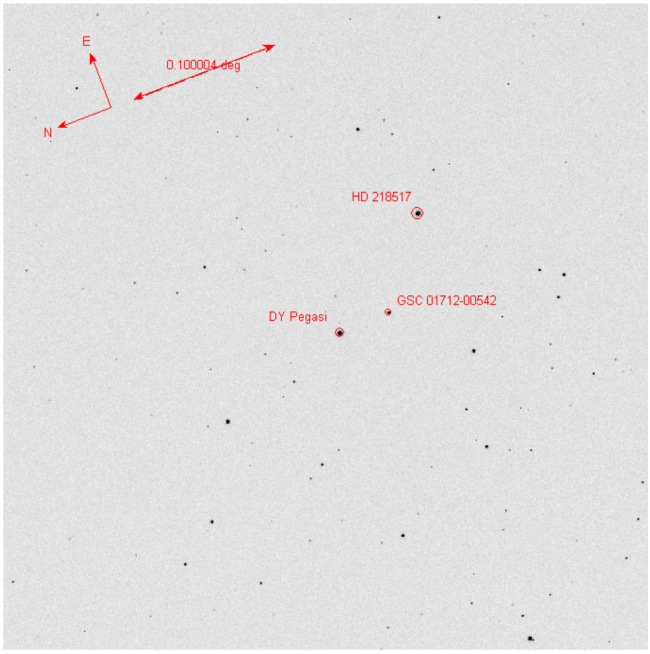

Figure 1. CCD Image of DY Pegasi and the calibration stars.

3. DATA REDUCTION

Calibrating the images was very straightforward. We took the median of the series of darks for our science images to obtain the science masterdark. We repeat this with the darks for the V flats and the darks with the B flats to obtain masterdarks for the V flats and B flats, respectively. We subtracted the science masterdark from each of our science images. The final result is 518 science images that are dark and flat corrected.

We astrometrically solved our images using the Astrometric Stacking Program (ASTAP) by Han (2022). Now there is a WCS mapped to each of our images, which is needed for source extraction.

We used the Python library for Source Extraction and Photometry (SEP) by Barbary (2016), which is an im-

plementation of Source Extractor (Bertin & Arnouts 1996) in Python, to detect and calculate the flux and flux error for every star in our images. To calculate the flux of each star, we used a circle with a radius of 6 pixels, which is sufficient for even the brightest stars in the image. This is shown in Figure 2. One thing to note was that even after dark-correction, there was a background count slightly above zero throughout the science images. This is the sky background. We were able to use SEP's on the fly local background subtraction to remove these background counts. A more detailed demonstration of SEP can be found in Appendix A.

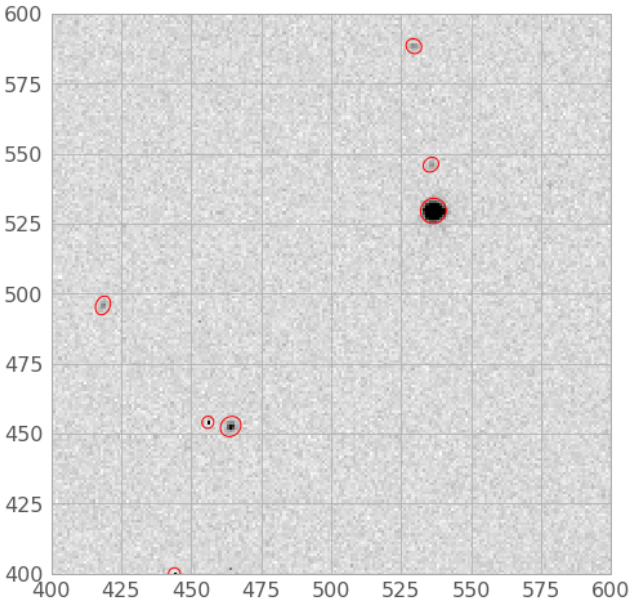

Figure 2. SEP output with a 6 pixel radius. The large star is DY Pegasi. In addition to extracting the center x and y coordinates, it also extracts the semimajor and semiminor axis (a and b) of elliptical objects. See the ellipse located near 425,500.

SEP calculates the flux and flux error values that corresponded to DY Pegasi and the calibration stars for each science image We plot the counts over time in Figure 3.

We convert the flux counts into an apparent magnitude. This is done using the calibration stars mentioned earlier. We use HD 218587 to calibrate for the B magnitude and GSC 01712-00542 to calibrate for the V magnitude. The V and B magnitudes of these stars were obtained from the AAVSO's APASS catalog (Henden et al. 2015), which is intended for the purposes of photometric calibration. We arrive at our final light curve of DY Peg in Figure 4, with uncertainties shown in Figure 5.

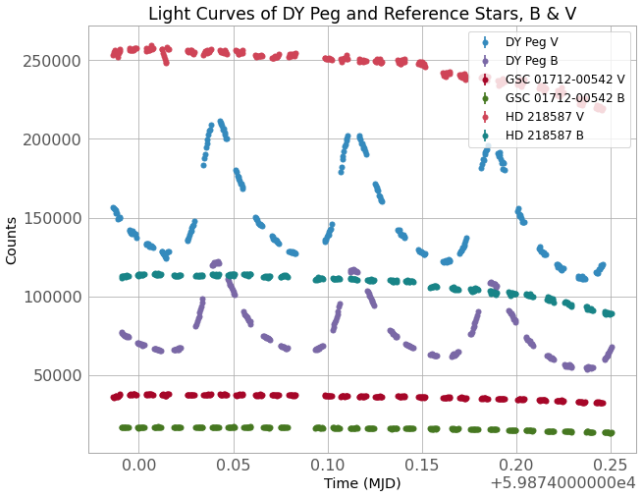

Figure 3. Flux of DY Pegasi and the calibration stars HD 218587 and GSC 01712-00542. The light curve of DY Pegasi clearly stands out from the other stars. We also see the alternating between B and V, as well as the observation gap due to the meridian flip.

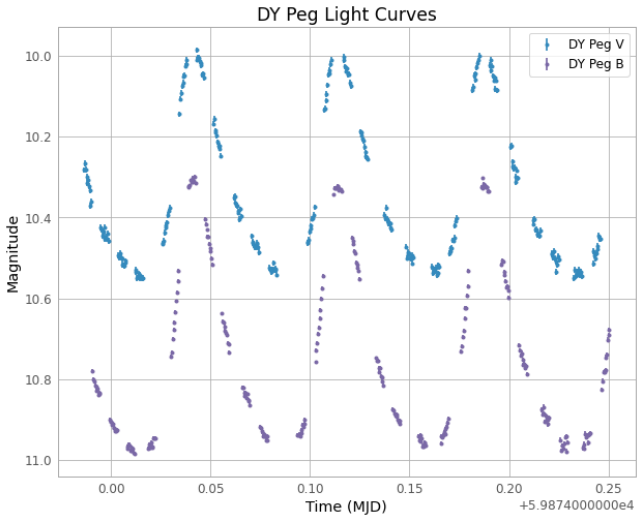

Figure 4. Final Light Curve of DY Peg ready for analysis.

4. DATA ANALYSIS & RESULTS

4.1. *Period*

In signal processing, the Fast Fourier Transform (FFT) is a powerful tool used to find the constituent frequencies that make up some unknown, periodic signal. One problem with using the FFT for the analysis of variable stars is that it requires evenly spaced data, which is often not possible (data often has gaps, or variance in the spacing). Interpolation would be required, but this is not a trivial task.

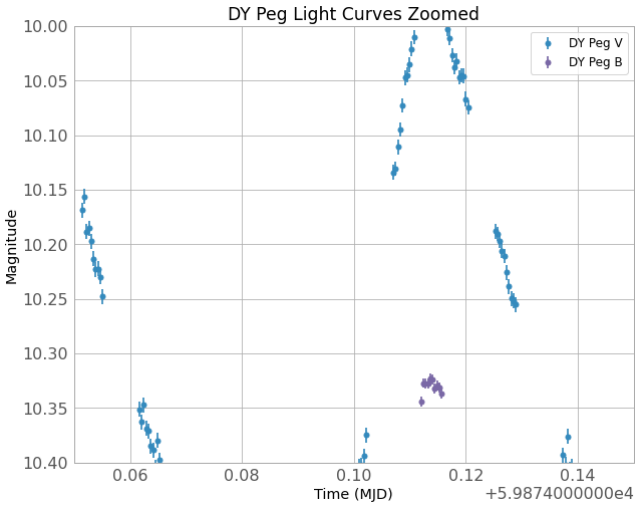

Figure 5. Zoomed in version of Figure 3. We can see the uncertainties are on the order of 0.01 mag.

Fortunately, the Lomb-Scargle Periodogram (LS Periodogram) was developed by Lomb (1976) and Scargle (1982) to allow frequency analysis of variable stars; it uses a regression to fit sinusoids to the data and has become a well-used tool for the analysis of variable star light curves. In this paper, we use the Period detection and Identification Pipeline Suite (PIPS), which is a recently developed, easy to use, and statistically robust Python package that allows for a similar analysis of light curves (Murakami et al. 2022).

PIPS addresses some shortcomings of the LS Periodogram, such as template bias to a sinusoid and uncertainty quantification. In a general sense, a χ^2 periodogram fits some model function to phase-folded data. The goodness-of-fit is then evaluated with the reduced χ^2 value. The LS periodogram, which is the most common implementation of a χ^2 periodogram in astrophysics, uses a sinusoid as its model function. Thus, results from a LS periodogram may differ from the true value if the signal is non-sinusoidal. This phenomenon is known as template bias. Additionally, LS periodograms can only infer the period, and uncertainties must be obtained through alternative means. These include the half-width at half-maximum (HWHM) of the peak spectral density, or through Markov Chain Monte Carlo (MCMC) or linear regression methods. As noted by Murakami et al. (2022), HWHM appears reasonable, but provides inaccurate results, and VanderPlas (2018) suggests to avoid this method. MCMC and linear regression provide more accurate uncertainty estimates, but are statistically and computationally more complex, making them less accessible. Although the template bias does not severely affect our analysis (pulsating variables are well described by multi-term sinusoids), the uncertainty provided by the PIPS package is very useful, as we will show.

PIPS uses a "Fourier likelihood periodogram", which is an alternate representation of a χ^2 periodogram. This novel approach converts the aforementioned χ^2 values to Gaussian likelihoods for each data point. Then, the product of the likelihoods is taken across all the data points. Mathematically, the likelihood of a given "test" period being the true period is:

$$\mathcal{L}(P_{\text{test}}, x, y, \sigma_y) = \prod_{i=1}^{N_{\text{data}}} \frac{1}{\sigma_i\sqrt{2\pi}} \exp\left[-\frac{(y_i - y_{i,\text{fit}})^2}{2\sigma_i^2}\right] \propto \exp\left(-\frac{1}{2}\sum_i \chi^2\right) \tag{1}$$

By calculating the likelihood for a range of test periods, PIPS creates its likelihood periodogram, where the y-axis represents a probability density function (PDF) instead of a spectral density function like in χ^2 periodograms. A Gaussian is fitted to the peak of the PDF, and PIPS uses the properties of the Gaussian to determine the uncertainty of the period. This is shown in figure 6 and figure 7.

As variable stars tend to have sweeping changes in brightness (as opposed to sharp changes like in an exoplanet transit, for example), the literature conventionally uses a multi-term Fourier series of the form

$$y_{\text{fit}}(x, P_{\text{test}}) = A_0 + \sum_{k=1}^{K_{\max}} \left[a_k \cos\left(\frac{2\pi k}{P_{\text{test}}}x\right) + b_k \sin\left(\frac{2\pi k}{P_{\text{test}}}x\right)\right] \tag{2}$$

to approximate light curves. In our data reduction we chose $K_{\max} = 5$, i.e. a 5-term Fourier series, as recommended by Murakami et al. (2022). PIPS optimizes the free parameters A_0, a_k, b_k to best match the phase-folded light curve. Increasing the number of terms allows better approximation to sharper peaks, but makes the fit more sensitive to noise. Decreasing the number of terms allows for worse approximation of sharper features, but makes the fit less sensitive to noise. The 5-term Fourier strikes a balance and provides the best results. We plot this 5-term Fourier solution with our phase-folded light curve in Figure 8.

DY Pegasi is known to have a second and third harmonic Xue & Niu (2020). Although this was not detected due in our limited observation run (Xue & Niu

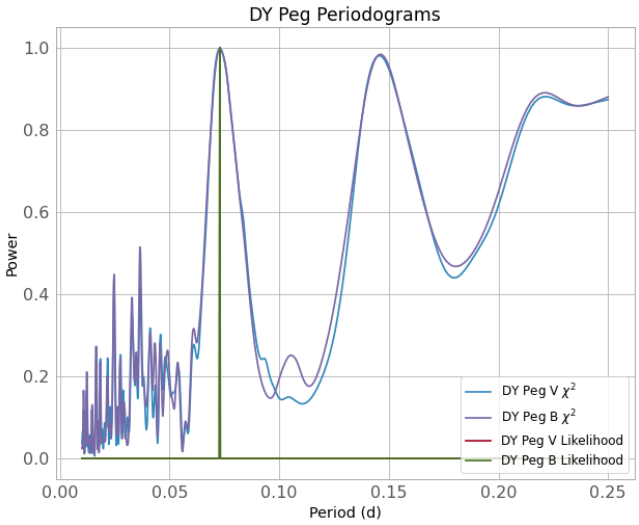

Figure 6. A χ^2 and Likelihood periodogram of DY Pegasi - the x-axis represents "guesses" of the period. For the χ^2 periodogram, the y-axis represents the spectral density, normalized to 1. High power for the χ^2 periodogram indicates the frequency associated with that period is detected with high confidence. The noisy spikes below 0.05 d are false positives from noise and the fact that our images were taken roughly 30 s apart. The peak at 0.07 d is the strongest peak, indicating that it is the period. The peak at 0.14 d is an integer multiple of 0.07 d, as is the one at 0.21 d. The tail that stretches to 0.25 d and beyond is an artifact of our observations taking place over the course of about 6 hours. Observations spread out over longer periods of time would reduce this tail. See Figure 7 for a close-up of the Likelihood periodogram, which is the spike centered at 0.7 d.

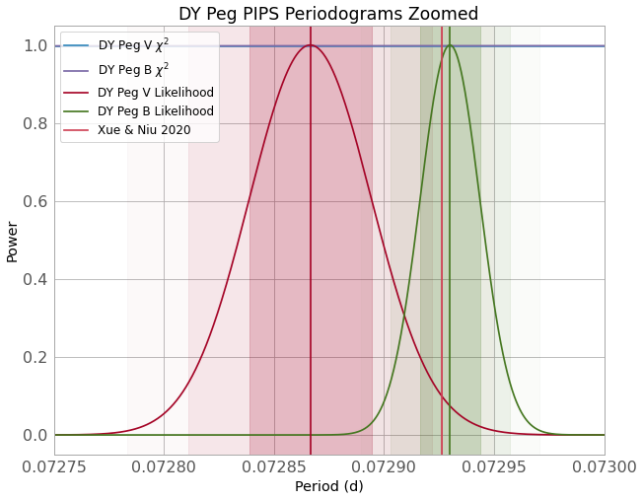

Figure 7. Zoom of Likelihood periodogram of DY Pegasi - the x-axis represents "guesses" of the period. For the likelihood periodogram, the y-axis represents the probability density, normalized to 1. High power for the likelihood periodogram indicates the frequency associated with that period is likely the true frequency. The vertical spans are a $\pm 1\sigma$ uncertainty centered around the predicted period. The peach-colored vertical line is the predicted period from Xue & Niu (2020), and their associated σ is less than the width of the line.

used several days of observations over the course of a month from the AAVSO database), these harmonics would cause a slow modulation of the periods over time. The 2nd harmonic is known to be small ($\approx 2\%$ the amplitude) compared to the first harmonic, but this could still result in subtle differences between periods. These differences would appear as discontinuities in a phase-folded plot if the difference is apparent at the beginning or end of the observation run, and this is what we believe to be causing the subtle "line-break" in the V plot at phase 0.75 and B plot at phase 0.85.

Using the aforementioned PIPS likelihood periodogram, We find the period in V to be 0.072867 ± 0.000028 d. The period in B was found to be 0.072929 ± 0.000014 d, as shown on Figure 7. These uncertainties are on the order of about 1 second, and they agree with each other within $\approx 1.5\sigma$. We believe the discrepancy arises from the less accurate V band. Although we would expect the V band to be more accurate due to higher counts, due to the timing of our image series, the V band was never able to capture the peaks of the periods, while the B band was able to capture the peak of all 3 periods. This would also explain why the uncertainty of the B band is half that of the V band. Our results in the B band agree with the literature value of $0.07292621 \pm 0.00000005$ d (Xue & Niu 2020) well within 1σ, while our V band agrees within $\approx 2\sigma$.

4.2. *Apparent Magnitude and Distance*

From the phase-folded plots in Figure 8, we find that the apparent V magnitude varies between 9.99 and 10.54. We can find the absolute V magnitude of DY Pegasi from the SX-Phoenicis Period-Luminosity Relation (Cohen & Sarajedini 2011):

$$M_V = -1.640(\pm 0.11) - 3.389(\pm 0.09) \log P \quad (3)$$

Substituting P, we find $M_V = 2.21 \pm 0.15$. the average apparent V magnitude by finding the average of Fourier solution in the phase-folded plot. It is $V = 10.3314 \pm 0.0002$. We use the distance modulus equation when taking galactic dust extinction into account:

$$d = 10^{\frac{1}{5}(m - M - A_V + 5)} \quad (4)$$

$$\sigma_d = \frac{d \ln 10}{5} \sqrt{\sigma_m^2 + \sigma_M^2} \quad (5)$$

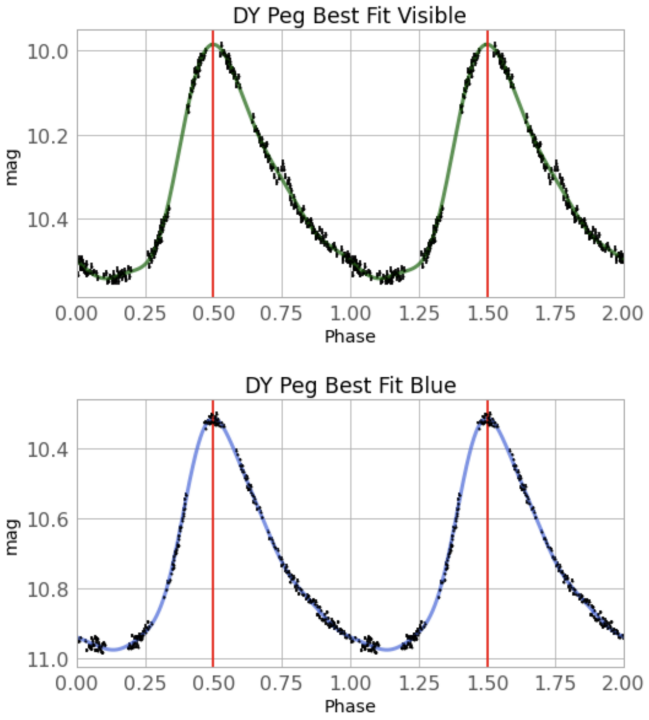

Figure 8. Phase-folded plots of DY Pegasi - We fold our 3 periods of data into a single phase, where the separation between the phases 0 and 1 is equal to the detected period. The fitted line is the 5-term Fourier solution found previously. The vertical red lines indicate peak magnitude. Note the small visual discontinuities at phase 0.75 for V and 0.85 for B. These could be due to the known second harmonic frequency that resulted in slight offsets over the three periods.

Here, $A_V = 0.411$ from the extinction maps by Schlegel et al. (1998). Hence, we find DY Peg's distance from Earth to be $d = 348 \pm 24$ pc.

Our distance agrees with the Gaia parallax measurement of 407 ± 7 pc (Gaia Collaboration et al. 2018) to within $\approx 2\sigma$. We believe the difference could arise from the second and third harmonics mentioned earlier. As the harmonics have different frequencies, it may take many cycles for the harmonics to constructively interfere to increase or decrease the magnitude of DY Pegasi. If we assume that DY Pegasi was brighter during our observation run and add 0.1 mag to our average apparent magnitude measurement of 10.33, we find the distance to DY Pegasi becomes 364 ± 24 pc, which is 0.7σ closer to the Gaia value.

4.3. *Bolometric Magnitude*

Later in the paper, we will make use of stellar evolution plots, which are typically calculated in units of $\log(L/L_\odot)$ and $\log(T(K))$. Here, L is the bolometric luminosity, which can be obtained from the absolute bolometric magnitude. We find the absolute bolometric magnitude of DY Pegasi by taking a bolometric correction of DY Pegasi from an empirical relation of δ Scuti variable stars (Petersen & Christensen-Dalsgaard 1999) (the category that SX Phoenicis variables belong to), and adding it to M_V. The bolometric correction relation is:

$$BC = 0.128 \log P + 0.022 \tag{6}$$

Substituting DY Pegasi results in $BC = -0.12$. Thus, we find:

$$M_{\rm bol} = M_V + BC = 2.09 \pm 0.15 \tag{7}$$

This is converted to luminosity in solar units, where $M_{\rm bol,\odot} = 4.73$.

4.4. *B–V Color Index and Spectral Type*

From the phase-folded light curves, we have a B and a V curve, as seen in Figure 8. By subtracting V from B and subtracting an extinction correction, E(B–V)= 0.133 found using the extinction maps from Schlegel et al. (1998), we obtain the B–V color index curve, shown in Figure 9. This figure clearly shows that DY Pegasi's color changes over the course of its period.

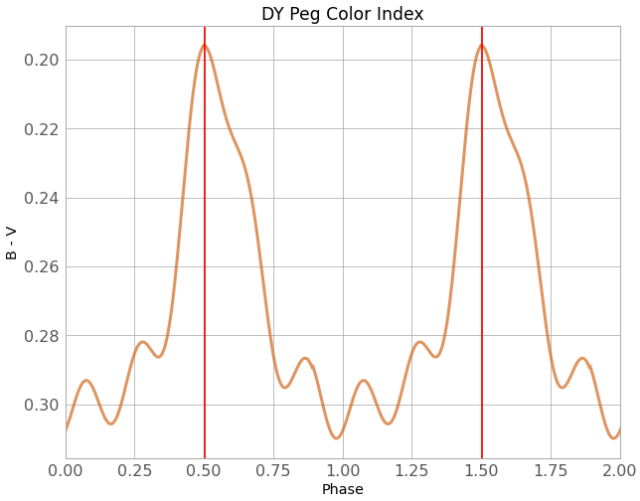

Figure 9. B−V Color Index - At peak brightness, the star has a lower B–V value. This indicates that the star is slightly bluer (recall lower magnitudes are brighter) when it is brighter, and slightly redder when it is dimmer.

The color index varies between 0.31 and 0.19. We can estimate the spectral type of DY Peg to vary between A9.5 at its dimmest and A6.5 at its brightest, based on the color index to spectral type conversion from Fitzgerald (1970).

We have different data points for B and V bands, since we could only take observations in one band at a time

and alternated every 5 minutes. Due to these 2 different sets of data points, our Fourier fitted line differs slightly from the B light curve to the V light curve. With our 5-term Fourier series, we capture the overall trend of the light curve correctly for both curves and obtain a precise period. The downside is that there will be some slight overfitting. This overfitting is not perceptible in Figure 8. However when we obtain the color index in Figure 9, we see smaller bumps that are likely from the differences in the Fourier solutions (overfitting) rather than intrinsic to the star. However, these charts are not meant to be very precise (we do not quote an uncertainty for these measurements, and neither does much of the literature). Rather, they are meant to be numbers in the same range as the literature. As mentioned in (Murakami et al. 2022) using a Fourier model with a low number of terms would result in a reduction in period detection accuracy, while using many more terms than 5 would likely result in more severe overfitting. The 5-term model was found to be the optimal model in their tests, providing the largest success rate (within 0.5% the true period).

4.5. *Temperature*

As color Index is related to temperature, since DY Pegasi's color index varies throughout its period, we expect its temperature to do so as well. Indeed, the color index curve can be converted to a temperature curve in Kelvin using Ballesteros's Formula (Ballesteros 2012):

$$T = 4600\left[\frac{1}{0.92(B-V)+1.7}+\frac{1}{0.92(B-V)+0.62}\right] \tag{8}$$

We convert the color index curve to a temperature curve and found it to range from $[7399, 8194]$ K, which falls very well in line with other literature values of $[7330, 8230]$ K (Hintz et al. 2004). The temperature curve is shown in Figure 10.

Considering Figures 8, 9, 10, we can see that when the star is at its brightest, it is at its bluest and hottest. When the star is dimmer, it is less blue and cooler. These changes are expected from the behavior of blackbodies. Recall that SX Phoenicis variables are a category of pulsating variable stars. While most main sequence stars are in a state of hydrostatic equilibrium, pulsating variables move between contracting and expanding periodically. Although the star reaches states that would be hydrostatic equilibrium, since the star was contracting or expanding, the outer layers have momentum that makes the star "overshoot".

4.6. *Mass*

Finally, we convert the apparent V light curve from units of magnitude into units of bolometric solar luminosities using the same process as for converting the apparent V magnitude to bolometric luminosity). We take the log of the bolometric luminosity and take the log of the temperature curve. We can plot $\log L/L_\odot$ vs. $\log T$, along with several stellar evolution tracks from the Geneva stellar evolution codes (Georgy et al. 2013). We plot tracks for a star with a metallicity of -0.8 dex or Z = 0.002 and rotational velocity of 23.6 km/s, which are consistent with the values of DY Peg from Cohen & Sarajedini (2011) and Solano & Fernley (1997), respectively. We also overlay the track of DY Pegasi as it varies throughout its cycle, and show the final graph in Figure 11.

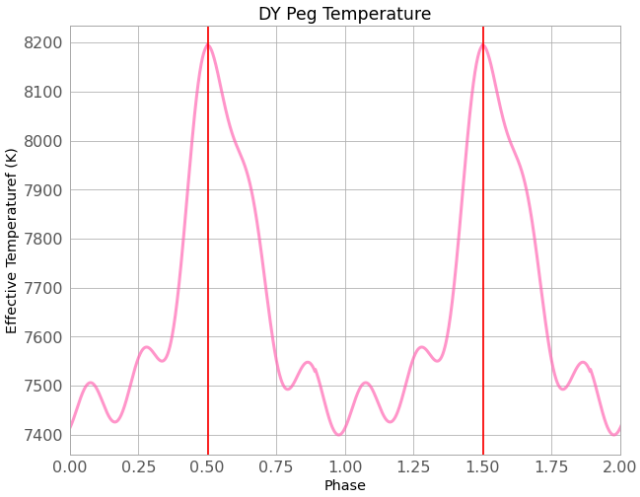

Figure 10. Temperature

Based purely on photometric observations, it would appear DY Peg should have a mass of about 1.3 $M_\odot$ and is entering the subgiant phase of its life. A feature that is ubiquitous in the stellar evolution of medium-mass stars ($1-10$ solar masses) is that there is a "hook" that separates the main-sequence and subgiant stage of the stars life. We see the hook in each of the stellar evolution plots toward the bottom left of the tracks Figure 11. Before the hook, the star evolves slowly, over billions of years. Once the star begins to exhaust its hydrogen, it contracts as a final attempt to maintain energy production in the core. The contraction results in higher temperatures, causing the hook to the left. This only works for a short time, and afterwards the star steadily migrates rightward along the HR diagram as a subgiant. Since DY Pegasi exists to the right of the hook, it would appear to be in the subgiant phase.

Our mass estimate is consistent with a star of its spectral type, and is close to the estimate of 1.5 $M_\odot$ by Hintz et al. (2004). However, we argue that because Hintz et al. (2004) uses stellar tracks with a much higher

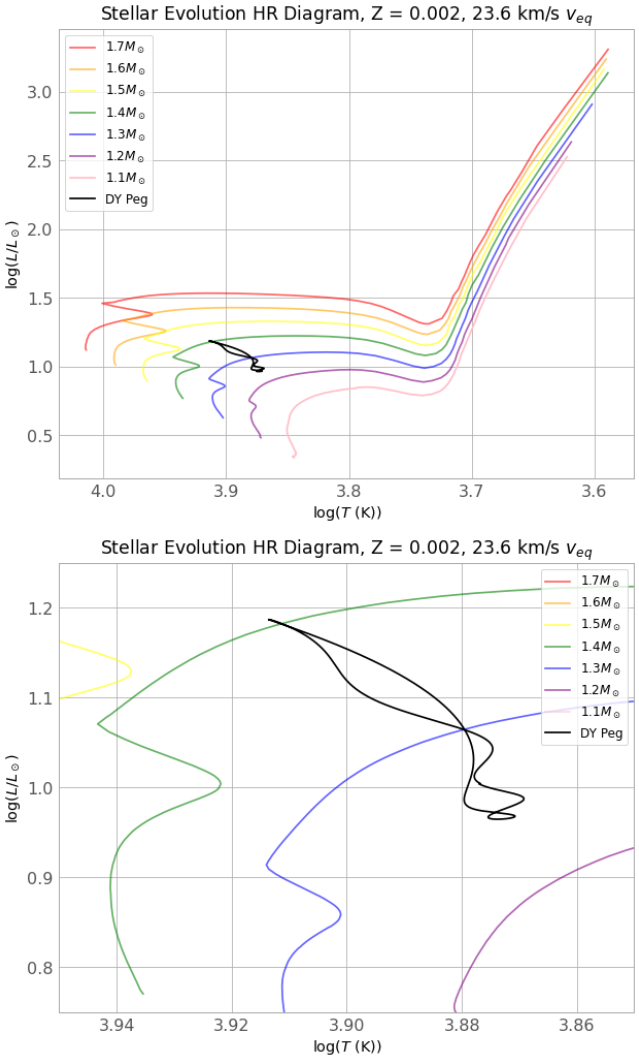

Figure 11. DY Peg and Some Stellar Tracks

metallicity of Z = 0.008, their value is possibly less accurate than ours. They do, in fact, obtain DY Pegasi's metallicity of Z = 0.002, but it is possible stellar evolution tracks for low metallicity stars did not exist at the time, and they had to use the Z = 0.008 tracks. Our photometric measurements are similar to theirs, so we believe if they used correct low metallicity tracks of Z = 0.002, they would have obtained a mass of about 1.3 $M_\odot$ as well.

However, our mass estimate is based purely off of our photometric measurements. The analysis by Xue & Niu (2020) finds a discrepancy between the photometric measurements (which are similar to ours) and the ratio between the first and second harmonic frequencies. Basically, the ratio between the first and second harmonic suggests that the mass of the star should be closer to 1 $M_\odot$, while their photometric results indicate the mass should be closer to what we obtained ($\approx 1.3 M_\odot$). It is known that DY Pegasi is in a binary configuration with another body. The orbital period is over 40 years, which means they are separated by a large distance. Given this information, they infer that this companion may be a white dwarf whose light is contributing some effect to the temperature and luminosity of DY Pegasi. This would relieve the discrepancy. There is additional supporting evidence for this theory: a spectroscopic analysis of DY Pegasi indicates an excess of calcium, sulfur, and carbon (Hintz et al. 2004), which are elements only formed in the asymptotic red giant branch. Thus, they believe that the "hidden" companion was once a main sequence star that became a red giant, died, and transitioned to a white dwarf. After expelling its outer layers, the excess metals accreted onto DY Pegasi. As the orbital period is quite long, no mass would have been transferred prior to the death of the binary companion (e.g. no envelope transfer). Finally, they argue that further measurements should be taken and whether this possible evolutionary history is common to all SX Phoenicis stars should also be tested.

5. CONCLUSION

In summary, after taking 3 periods of DY Pegasi at Mt. Stony Brook Observatory, we have found its period, magnitude, luminosity, distance, color index, temperature, and estimated its mass from matching the photometric measurements with stellar evolution plots. We found the distance of 343 ± 24 pc to be close to the Gaia value 404 ± 7 pc, its spectral type to vary between A6.5–A9.5, its temperature to range between $[7399, 8194]$ K, and its mass to be approximately 1.3 $M_\odot$ from photometric measurements alone.

6. ACKNOWLEDGEMENTS

The author thanks Mark Vincent Guevarra and Henry Shi for their assistance on the night of data acquisition, as well as their feedback that improved various parts of the data analysis. The author also thanks Dr. Von der Linden for her guidance throughout the research process, and for her feedback that improved the quality of this paper. Finally, the author thanks Ben Levine and Aaron Mueninghoff and for their help on the night of data acquisition and assistance during data reduction.

REFERENCES

Ballesteros, F. J. 2012, EPL (Europhysics Letters), 97, 34008, doi: 10.1209/0295-5075/97/34008

Barbary, K. 2016, Journal of Open Source Software, 1, 58, doi: 10.21105/joss.00058

Bertin, E., & Arnouts, S. 1996, A&AS, 117, 393, doi: 10.1051/aas:1996164

Cohen, R. E., & Sarajedini, A. 2011, Monthly Notices of the Royal Astronomical Society, 419, 342, doi: 10.1111/j.1365-2966.2011.19697.x

Fitzgerald, M. P. 1970, A&A, 4, 234

Gaia Collaboration, Brown, A. G. A., Vallenari, A., et al. 2018, A&A, 616, A1, doi: 10.1051/0004-6361/201833051

Georgy, C., Ekström, S., Eggenberger, P., et al. 2013, A&A, 558, A103, doi: 10.1051/0004-6361/201322178

Han. 2022, Astrometric Stacking Program. https://www.hnsky.org/astap.htm

Henden, A. A., Levine, S., Terrell, D., & Welch, D. L. 2015, in American Astronomical Society Meeting Abstracts, Vol. 225, American Astronomical Society Meeting Abstracts #225, 336.16

Hintz, E. G., Joner, M. D., Ivanushkina, M., & Pilachowski, C. A. 2004, PASP, 116, 543, doi: 10.1086/420858

Lomb, N. R. 1976, Ap&SS, 39, 447, doi: 10.1007/BF00648343

Murakami, Y. S., Jennings, C., Hoffman, A. M., et al. 2022, MNRAS, 514, 4489, doi: 10.1093/mnras/stac1538

Petersen, J. O., & Christensen-Dalsgaard, J. 1999, A&A, 352, 547

Rodríguez, E., & López-González, M. J. 2000, A&A, 359, 597

Scargle, J. D. 1982, ApJ, 263, 835, doi: 10.1086/160554

Schlegel, D. J., Finkbeiner, D. P., & Davis, M. 1998, ApJ, 500, 525, doi: 10.1086/305772

Solano, E., & Fernley, J. 1997, A&AS, 122, 131, doi: 10.1051/aas:1997329

VanderPlas, J. T. 2018, ApJS, 236, 16, doi: 10.3847/1538-4365/aab766

Xue, H.-F., & Niu, J.-S. 2020, ApJ, 904, 5, doi: 10.3847/1538-4357/abbc12

APPENDIX

A. DEMONSTRATION OF SEP

Consider the following image from our observation run:

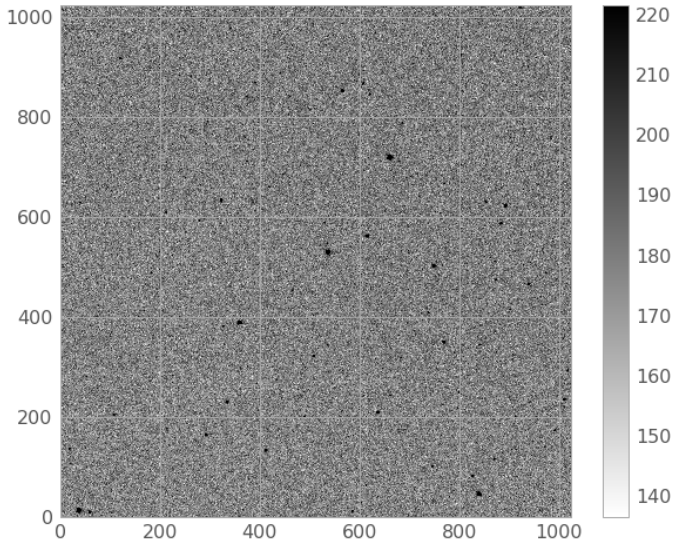

Figure 12. A typical image in the V band

We can see that the typical counts are approximately 425 based on the scale. Indeed, if we print the background and background RMS error we see this.

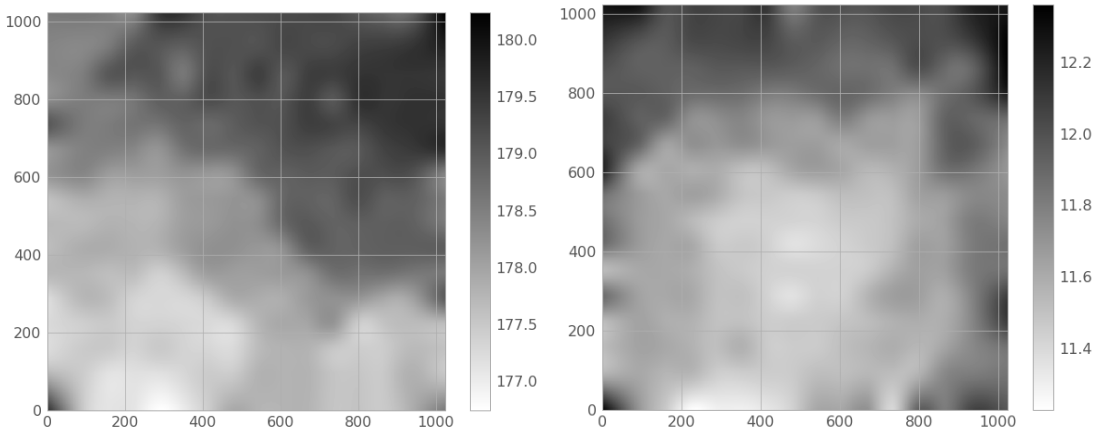

Figure 13. The background and background error of Figure 3, respectively.

We can simply subtract the background from our original image. The error will stay the same, and this is used to source extract the stars. One of the parameters for star detection is a threshold of sigma, which is based off the background error.

We can source extract the stars in Figure 11 and draw an ellipse around each detected object. In Source Extractor, a catalog data file would be outputted. In SEP, the "catalog" is instead stored in-memory. We draw the ellipses by retrieving the x-coordinate, y-coordinate, ellipse semi-minor and semi-major axis, and ellipse angle. For stars, this

ellipse should be almost exactly a circle. However, we do spot at least one galaxy in the image, as it has an elliptical shape near pixel coordinates (400,600).

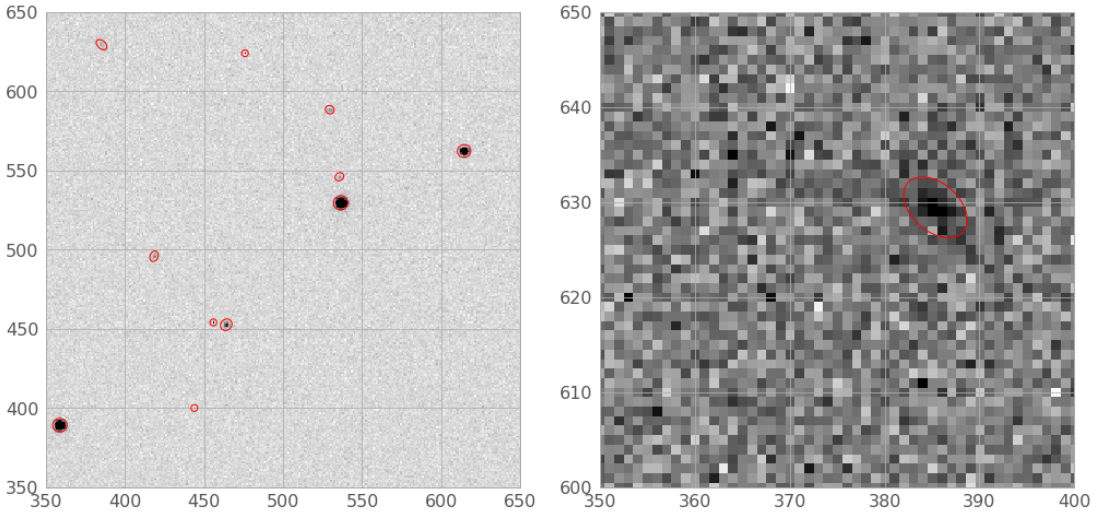

Figure 14. Source extraction of the image. Notice the galaxy located near 400, 600.

From here, we would simply retrieve the desired flux counts. In the same way that we can retrieve the x and y coordinates, we can retrieve flux and flux error.